2008 IEEE International Conference on
Robotics and Automation
Pasadena, CA, USA, May 19-23, 2008

Towards a Needle Driver Robot for Radiofrequency Ablation of Tumors under Continuous MRI††

Rebecca Kokes*, Kevin Lister*, Rao Gullapalli† (PhD), Bao Zhang†, Howard Richard† (MD), Jaydev P. Desai*[1] (PhD)
*Robotics, Automation, Manipulation, and Sensing (RAMS) Laboratory, University of Maryland, College Park, USA
†University of Maryland School of Medicine, Baltimore, USA

Abstract— **This paper presents an initial design and feasibility study for a 1-DOF Magnetic Resonance Imaging (MRI) compatible needle driver robot for radiofrequency ablation (RFA). This initial design and study is necessary to further understand how to improve on many of the shortcomings in the standard RFA procedure. Combining needle driving with advanced image tracking techniques could provide improved solutions to these clinical limitations. In this paper, we present a hydraulically-actuated 1-DOF needle driver robot that is capable of advancing a radiofrequency (RF) probe into tissue at controllable velocities and positions within an MRI scanner, while collecting force feedback data and maintaining all standards of MRI-compatible design. We also present a method of interfacing the robot with a PHANToM haptic feedback device controlled from outside the MRI scanning room. Experiments demonstrating the PHANToM's ability to receive force feedback and guide the RFA tool to a tumor nodule within a phantom breast model while continuously imaging within MRI have been presented. Our haptic feedback system enabled us to detect normal vs. tumor phantom tissue in the preliminary experiments. Our experimental results demonstrate the compatibility of the entire system for operation during continuous MRI imaging.**

Keywords— Medical robotics for RF ablation; Haptic feedback; Continuous MRI imaging; Teleoperation.

I. INTRODUCTION

Radiofrequency (RF) ablation is a needle-based cancer treatment procedure in which the tumor is ablated *in situ* through the use of a needle electrode that is inserted percutaneously into the tumor. RF current is passed through the electrode or set of electrodes, heating the tumor until tissue necrosis occurs [1-4]. This promising medical technique has become a popular treatment for primary and secondary liver tumors as an alternative to standard surgical procedures. In recent years it has also been applied to primary tumors in the breast, kidney, bone, adrenal glands, and lung [1]. While RFA has achieved wide success in recent years, the conventional procedure still exhibits many shortcomings. A clinical study for RFA of liver tumors reports a full necrosis rate of 95.1% of the treated tumors [5], while initial studies for RFA of breast cancer report that in order to reach high success rates a volume much bigger than the tumor must be ablated, unnecessarily damaging healthy tissue [6]. Meanwhile, reported short-term disease-free survival rates for those treated with RFA for liver cancer vary from around 80% [5, 7] to 54.6% [8]. Potential reasons for the somewhat limited success of RFA stem from uncertainties in imaging technology, human error in probe placement, movement of the chest and abdomen through the normal respiratory cycle during probe placement, and unpredictable shape and volume of ablated tissue [6, 9].

However, one of the primary reasons for this recurrence is the limitation of accurately identifying tumor boundaries and monitoring tumor necrosis under Computed Tomography (CT) or Ultrasound (US) guidance. As a result, to ensure that the entire tumor is ablated, surgeons generally attempt to ablate a large margin of supposedly healthy tissue around the tumor, thereby increasing the probability that no cancerous tissue/cells are left post-ablation. Nonetheless, some cancerous cells are often over-looked, resulting in the above percentages of cancer recurrence, while a significant amount of healthy tissue is also ablated. Currently breast RFA is performed with Ultrasound guidance. This approach to guidance is limited, as RFA causes microbubbles to form in tissue. This leads to acoustic noise, which makes it difficult to image the lesion and accurately position the RFA probe or monitor tumor necrosis. MRI guidance provides an advantage over CT and US, in that it offers radiation-free imaging (unlike CT), sharper image contrast, and the ability to detect thermal gradients around the ablated region, which can potentially improve the probability of complete intended tumor ablation through temperature maps [10].

In recent years, a significant amount of research has been conducted to improve the success rate and applicability of RFA. In general, past research has concentrated on improving RF procedures to increase the volume of ablated tissue, or to decrease the duration of the ablation procedure [11, 12]. Meanwhile, the possibility of performing RFA under continuous MRI imaging has received significantly less attention within the engineering and medical communities. RFA-based procedures that are currently done using MRI are performed under "image guidance", where the procedure is performed after imaging, rather than under "continuous imaging", where the procedure is performed during imaging. Tele-operated RFA with continuous imaging could improve many of the shortcomings in the standard RFA procedure. One effort at such a device has been made by Bradford Wood et al, who have designed and implemented a CT-compatible robot for needle insertion [13, 14]. Activated by a pneumatic gripper, the device is capable

[1]Corresponding Author.

†† We would like to acknowledge the support of National Science Foundation grant CCF0704138 and NIH grant R01EB006615 for part of this work.

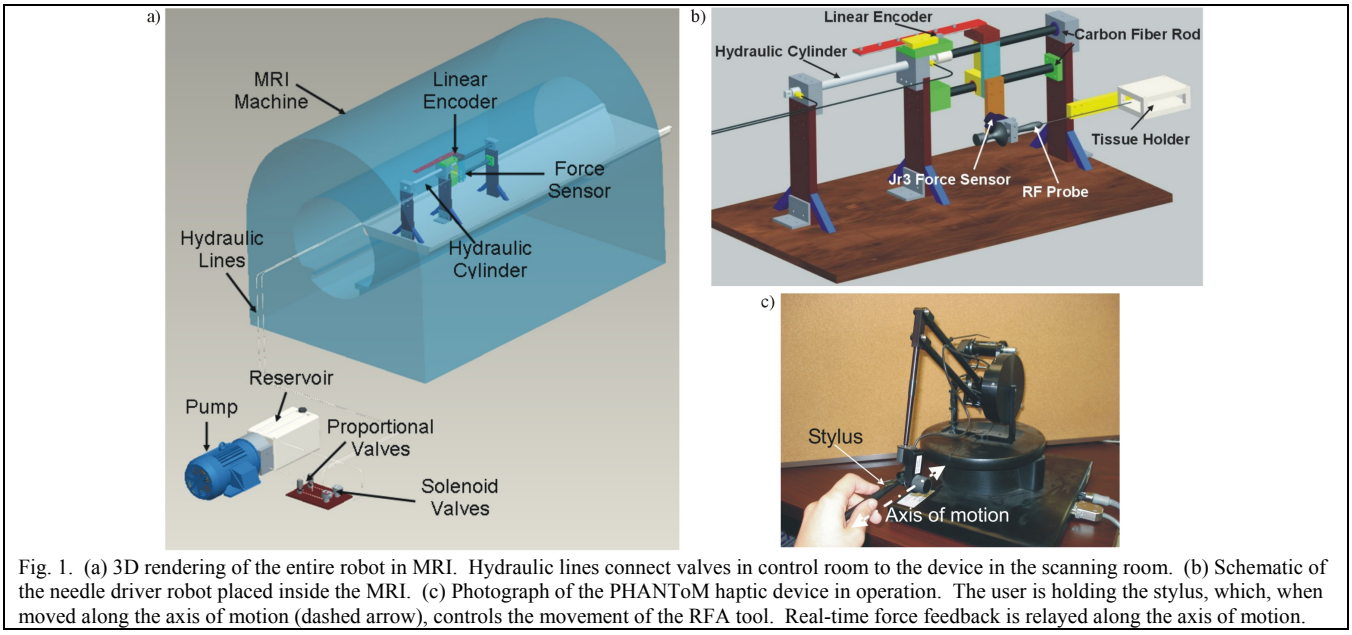

Fig. 1. (a) 3D rendering of the entire robot in MRI. Hydraulic lines connect valves in control room to the device in the scanning room. (b) Schematic of the needle driver robot placed inside the MRI. (c) Photograph of the PHANToM haptic device in operation. The user is holding the stylus, which, when moved along the axis of motion (dashed arrow), controls the movement of the RFA tool. Real-time force feedback is relayed along the axis of motion.

of advancing an RF probe inside a CT scanner, through either a semi-automated or fully automated process [15]. While this device has been successful within the CT environment, it has not been designed or implemented for use with MRI. Since needle tracking and tumor visualization have been shown to be far superior with MRI [16, 17], it is necessary to bring automation of RF probe placement to the MRI environment. Due to workspace constraints, this is facilitated through the use of a tele-operated device. While several robotic systems have been developed for MRI-guided needle insertion [18, 19], we are not aware of any for RFA under continuous MRI imaging.

The goal of this paper is to present the design of a prototype of a MRI-compatible 1-DOF robot for automated RF probe advancement with haptic feedback, along with a series of experiments proving MRI-compatibility and functionality of the device. While the current design is not suited for use with patients, it has been built to demonstrate the feasibility of such a device, as well as to conduct initial experiments that will assist with the design of a multi-degree of freedom robot for use in clinical practice. The primary advantage of our proposed robot is that it can perform the RFA procedure inside the scanner under continuous MRI.

This paper is divided into the following sections. In section II, we present the materials and methods used for the design and development of the 1-DOF robot. We also describe the haptic implementation platform, system modeling, experimental procedure for testing MRI-compatibility and the effectiveness of our teleoperated robotic system. In section III we present the results of our work, and finally, in section IV we present our conclusions and future work in this area.

II. Materials and Methods

A. Design and Development of a 1-DOF Robot

This device was designed to perform automated advancement of the RF probe inside the MRI scanner, while at the same time recording the forces exerted by the probe on the force sensor during insertion and withdrawal. The basic design constraint for the preliminary design was MRI-compatibility of the actuators, sensors, and structural components. To ensure MRI-compatibility, electro-hydraulics was chosen as a means of actuation, polypropylene was chosen as the main material for the structure of the device, and MRI-compatible sensors were used [20, 21]. With the exception of the optical encoder and the force sensor, all electronics and computer equipment are located in the control room to minimize noise, while the cables and hydraulic lines run into the scanning room through a copper-lined port, which attenuates the RF noise.

Structural / Motion Components: Fig. 1(a) shows the schematic of the overall system. Fig. 1(b) shows the device, which consists of several custom-machined polypropylene parts. The top carbon-fiber rod is coupled to the piston rod. The slider is clamped tightly to the top carbon-fiber rod, while it is free to move relative to the bottom carbon-fiber rod. In operation, as the piston rod extends, the top carbon-fiber rod and the slider move with it, advancing the RF probe. Meanwhile, the bottom carbon-fiber rod remains stationary, acting as a linear guide. In addition, a tissue clamp is attached to the rightmost support.

Hydraulic Components: The hydraulic system consists of two proportional valves, two solenoid valves, a hydraulic cylinder, a pressure regulator, and a hydraulic power unit. Since the valves and hydraulic power unit are not MRI-compatible, they are located in the control room, and hydraulic lines are taken to the main device in the scanning room.

The proportional valves (IQ Valves Mini PFCV, Part No. 209236) are responsible for controlling the flow into each port of the hydraulic cylinder. Proportional valve #1 (Fig. 2) controls piston motion in the forward direction, while proportional valve #2 controls piston motion in the reverse direction. The direct-acting poppet solenoid valves (Asco Valves Model No. 8262G002) are used to regulate the draining of hydraulic fluid into the reservoir. When proportional valve #1 is activated and the piston is moving forward, solenoid valve #2 is in the open position to

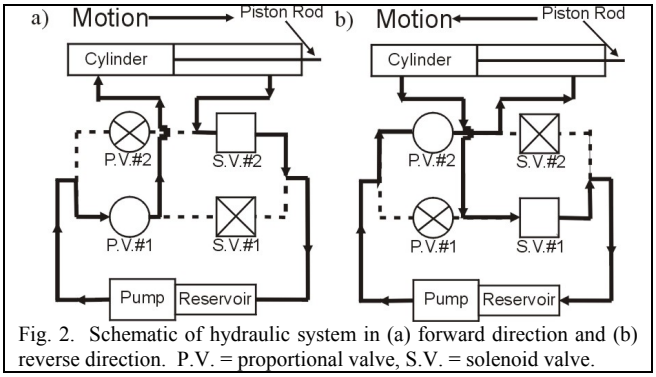

Fig. 2. Schematic of hydraulic system in (a) forward direction and (b) reverse direction. P.V. = proportional valve, S.V. = solenoid valve.

passively filter fluid from the cylinder's port back to the reservoir, while solenoid valve #1 is closed (Fig. 2(a)). Conversely, when proportional valve #2 is activated and the piston is retracting, solenoid valve #1 is in the open position while solenoid valve #2 is closed (Fig. 2(b)).

The hydraulic cylinder (Bimba All-Stainless Non-Repairable Original Line, SS-0412-DXPW) is made of stainless steel to ensure MRI-compatibility. However, MRI-compatibility does not ensure absence of artifacts in the image. The entire system has been designed so that the image components are within the scan field of the RF coil, while the other components, such as the cylinder and the force sensor, are outside the imaging area, but magnetically neutral.

Sensing and Control Components: The device is equipped with a MRI-compatible linear encoder acting as a position sensor for the needle traversal. The encoder head (US Digital Part No. EMI-0-500, 500LPI) is mounted to the top of the middle support of the device and remains stationary, while the linear strip (US Digital Part No. LIN-500-12, 500 LPI) is mobile and moves along with the slider, force sensor and RF probe. A PL5 differential line drive is utilized to increase the signal output due to the long connecting wire running out of the scanning room.

The force sensor (JR3 Model No. 20E12A-I25) is mounted to the force sensor plate on the slider. The RFA tool is then mounted to a plate directly on the force sensor surface, such that the sensor records the forces/torques that are experienced by the RF probe, in F_x, F_y, F_z, τ_x, τ_y, and τ_z, with a resolution of 0.002N in F_x, F_y, and F_z and 0.00025Nm in τ_x, τ_y, and τ_z. The force sensor has been custom-modified for MRI compatibility, with brass screws and hardwired cable (without an external connector). A dSPACE DS1103 controller board is used to record the position and force data from the sensors in real time, at a time step of 1ms. A PI control law is implemented to control the motion of the piston rod, slider, and RF probe.

Haptic Implementation: To enable haptic feedback, the dSPACE controller code was interfaced with a PHANToM haptic device (SensAble Technologies, Version 1.5A), operated in the control room (Fig. 1(c)). Probe motion is controlled in real-time by the motion of the PHANToM stylus, while data from the force sensor is relayed back to the stylus to generate real-time haptic feedback. Since the primary force sensing takes place along the x-axis of the force sensor, we displayed the x-component of the force through the PHANToM. This is a reasonable simplification since the majority of force should only be felt along the axis

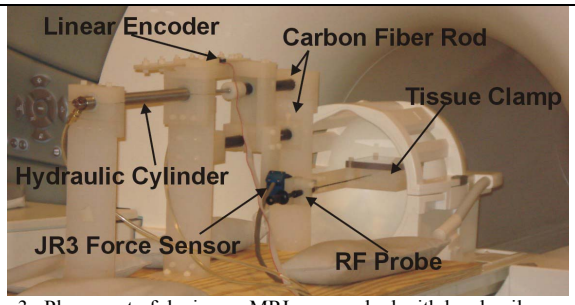

Fig. 3. Placement of device on MRI scanner bed with head coil.

of the RF probe. Force data from the sensor and velocity readings from the PHANToM stylus were filtered online with a 5th order Butterworth low-pass filter.

B. System Modeling and Controller Design

To fully understand the dynamic response of the hydraulic system and design a suitable PI controller, the device was modeled with the assistance of the Matlab System Identification Toolbox. A series of experiments were performed in which constant voltages were applied to the proportional valves in both the forward and reverse directions, and encoder data was recorded at a time step of 1ms to determine the velocity of the probe in response to each step input. Five experiments were performed for each direction, at 8V, 12V, 16V, 18V, and 20V. Data sets with voltage input and velocity output were imported into the System Identification Toolbox in Matlab. We chose to model the system as an over-damped second-order process model, whereby the transfer function in the s-domain took the following form:

$$G(s) = \frac{K}{1 + 2\zeta T_w s + T_w^2 s^2} e^{-T_d s} \quad (1)$$

where K is the static gain, T_w is the natural period, T_d is the time delay, and ζ is the damping coefficient, which is greater than 1. The toolbox then used the input/output relationship of the step response to generate a best-fit model, obtaining the values for the transfer function parameters. Models were re-iterated until at least a 75% fit was reached, verifying that the chosen model structure and selected parameters are adequate. The standard deviations for the parameters in each direction were obtained, and after verifying a narrow spread of data, the average value for each parameter was selected to create an average model.

After obtaining a suitable plant model for both forward and reverse motion of the hydraulic cylinder, each system was simulated in Simulink® as a hybrid block diagram with a discrete controller and analog plant, as seen in Fig.4. A proportional gain and an integral gain for the controller were selected for both forward and reverse.

C. Experimental Procedure for Demonstration of MRI-Compatibility

To determine the degree of MRI-compatibility, we used signal-to-noise ratio as a quantification of image disturbance, where SNR is defined as the ratio of the mean pixel value of the signal and the standard deviation of the pixel value of the background noise [22]. To do this, we placed the device in the scanner (Siemens Magnetom 1.5T)

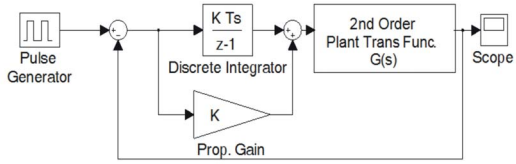

Fig. 4. Block diagram of closed-loop system.

with the RF probe inserted into a phantom breast tissue and scanned several images during a dynamic scan (Fig. 5). From the image, a small homogenous region was selected from the imaging area of the phantom tissue as the signal region of interest (ROI), while a large region from the background was selected as the noise ROI. From here, the SNR was calculated using image processing techniques in Matlab. This procedure was repeated for three images of varying qualities.

In addition to the noise studies, we also need to verify that the force sensor readings are not affected by the MRI. To determine the effect of MRI on force values, we obtained force profiles during probe insertion into a homogenous phantom tissue sample, both inside and outside the MRI. The force profiles were then qualitatively compared.

D. Experimental Procedure for Demonstration of Device Functionality

We first needed to verify that the PHANToM device can accurately control the position of the RF probe. To do this, we advanced and retracted the probe in the phantom tissue using the PHANToM stylus at approximately 0.5 cm/sec, once again both inside and outside the MRI. We then compared encoder data for the position of the RF probe with the position of the stylus at every time step, thus determining whether or not the device satisfactorily follows the stylus motion. In addition, we also verified that the correlation is the same both inside and outside the magnetic field. Position was used as an indicator of the PHANToM's ability to accurately control the needle motion, while moving at a constant velocity. In the future, it will also be helpful to evaluate the robot's response to varying velocity commands.

Another necessary experiment was to demonstrate the PHANToM's ability to guide the RF probe into a tumor, while continuously imaging the needle and tumor region and transmitting force feedback of the needle-tumor interaction to the haptic device. We used a phantom breast tissue with various MR-sensitive inclusions. While advancing and retracting the RF tool, we imaged the tumor region using a dynamic scan, which generated a sequence of images taken at a frame rate of 3.7 seconds, allowing us to track the motion of the needle. The MRI images were used to verify that the probe was inserted into the tumor, while the force profile along the axis of the RF probe was generated to analyze the haptic feedback due to the probe's contact with the tumor. We then used the frame rate of the dynamic scan to determine the time at which each image was taken, which allows us to compare the force profile to events in the images, such as needle insertion into the tumor. From here, we determined the robot's ability to detect the presence of a tumor via force feedback.

III. RESULTS

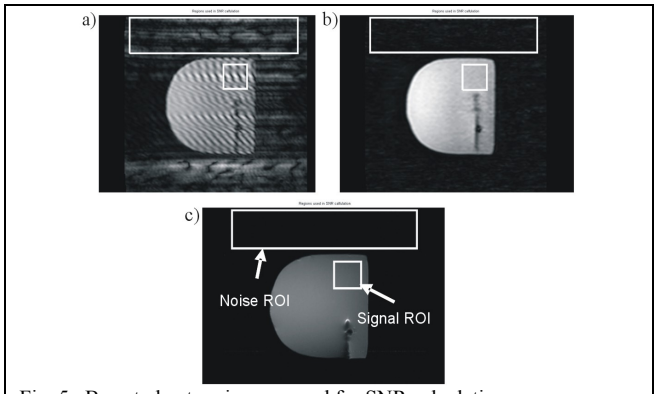

Fig. 5. Breast phantom images used for SNR calculation.

A. System Modeling and Controller Design

For the process models identified in Matlab relating input voltage to piston velocity, Table 1 summarizes the averaged parameters for each direction, along with the associated standard deviations. We see that the standard deviations are minimal enough to allow for averaged parameters to be used in Eq.1. These models were simulated in Simulink, and step response simulations were run until we achieved a steady state error of 0.1% and a rise time of 0.1 seconds. Based on these criteria, an integral gain of 300 was selected for both models, and proportional gains of 250 and 300 were selected for the forward and reverse directions, respectively.

TABLE 1. AVERAGE PARAMETERS FOR SECOND ORDER PROCESS MODEL

	Forward		Reverse	
	Avg.	St. Dev.	Avg.	St. Dev.
Damp. Coeff.	2.738	0.268	3.527	0.233
Static Gain	0.033	0.004	0.028	0.002
Nat. Period	0.180	0.019	0.204	0.073
Time Delay	0.000	0.000	0.000	0.000

B. MRI-Compatibility

After obtaining various images with the robot inside the scanner bore, no major artifacts were observed, and noise in the image was minimal (Fig. 5). We obtained a wide range of signal-to-noise ratios for the three tested images: 5.2 for Fig. 5(a), 21.0 for Fig. 5(b) and 106.7 for Fig. 5(c). Even the image with the worst quality (Fig. 5(a)) had an SNR of greater than 5. Therefore, from an imaging point of view, the robot is MRI-compatible and does not introduce an artifact in the image, enabling its usage within the MRI environment during continuous imaging.

We also generated Force vs. Displacement profiles to compare the force sensor readings both inside and outside the MRI. Figure 6(a) shows the force profile along the long axis of the RF probe (the x-axis). As seen in the figure, force readings in the x-direction are not significantly affected by the magnetic field. From Fig. 6(a), we see a high force of around 1.5 N at about 0.5 cm of travel. This value corresponds to the large build-up of force that occurs before the probe punctures the surface of the tissue sample. After this 1.5 N peak, we see that in both experiments the forces immediately drop below 0.5 N before slowly increasing as the depth of insertion increases, corresponding to the additional friction force that builds up as a higher surface area of the needle is in contact with the tissue.

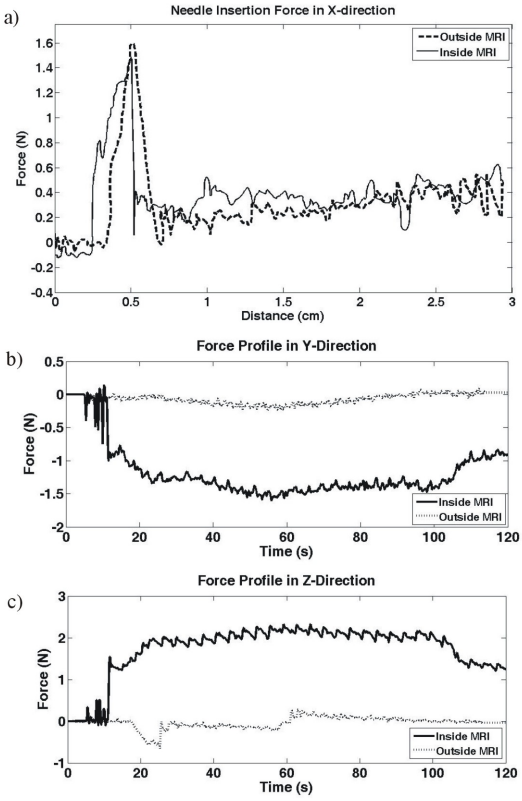

Fig. 6. Force profiles during needle insertion. a) Force in the X-direction vs. Displacement, b) Force in the Y-direction vs. Time, c) Force in the Z-direction vs. Time

Unfortunately, this degree of MRI-compatibility was not demonstrated for the forces in the y- and z-axes. Outside the MRI, F_y and F_z were negligible, which is what one would expect perpendicular to the direction of motion. However, inside the MRI, the force sensor generated noticeable negative forces in the y-axis (Fig. 6(b)), and noticeable positive forces in the z-axis (Fig. 6(c)). Given that the magnetic field pointed in the x-direction, it is logical that these forces were due to eddy currents that were induced as the force sensor traversed along the length of the magnet bore. Since the forces in the x-axis are parallel to the magnetic field, there is no induced current in this direction. However, since the y- and z-axis are perpendicular to the magnetic field, eddy currents could be induced, resulting in faulty force signals in these directions. As a result, we chose to display the x-directional force through the haptic feedback device, as that is a realistic representation of the force exerted on the force sensor by the probe.

C. Position Control with Haptic Device

Position profiles of the PHANToM stylus and the RF probe are shown in Fig. 7. As seen from the figure, the motion of the RF probe coincides well with the movement of the PHANToM stylus, demonstrating that the robot can be accurately controlled with the haptic device.

D. Needle Tracking and Force Feedback during RF Probe Insertion into Phantom Breast Tumor

A final test was conducted to determine if the device could detect the presence of an inclusion within a phantom breast model. The images from the dynamic scan verify that

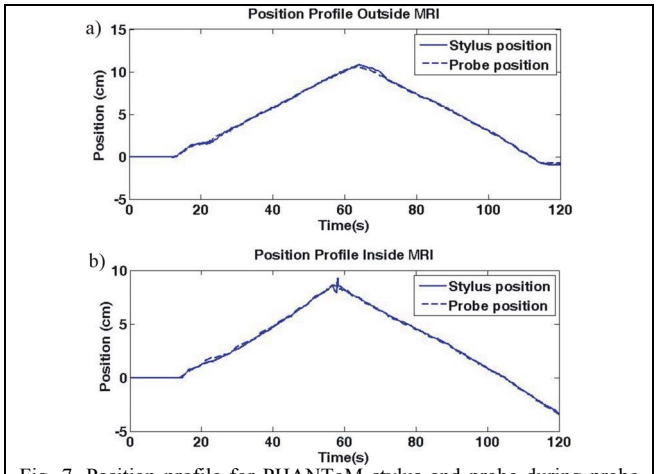

Fig. 7. Position profile for PHANToM stylus and probe during probe insertion and withdrawal (a) outside the MRI and (b) inside the MRI.

the needle did in fact pass through the inclusion of interest (Fig. 8 (b)-(e)). In addition, using the fact that the time between scans was 3.7 seconds, it is possible to determine the time at which the tip of the probe came in contact with the inclusion and the time at which it re-entered normal tissue. The time stamp of each image of interest is overlaid on the force profile (Fig. 8(a)). These times correspond to variations in the force profile that can be explained by the time of puncture and increases in friction force while the needle is within the inclusion. For example, at about 16.7 seconds we see a peak in the force profile corresponding with the image scanned at 16.7 seconds (Fig. 8(c)). At about 30.1 seconds, we see a large variation in the force profile, which corresponds to Figure 8(d), where the probe first begins to puncture the tumor. Finally, Figure 8(e) depicts the instant that the probe is retracting and exiting the tumor, which results in a noticeable change in the force profile. Based on these observations, we concluded that the user can in fact detect the presence of an inclusion through both visual and haptic feedback. Furthermore, we determined the qualitative changes in the force profile that occur as the RF probe interacts with a tumor during insertion. As seen in Fig. 8(a), insertion into the tumor results in a high-frequency and high-amplitude fluctuation in force, caused by the change in friction force and elasticity, as the probe is driven through the inclusion. Since the velocity of needle motion is shown to be fairly steady in Figure 7, we can conclude that the observed frequencies are due to contact with the tumor, rather than due to sudden variations in needle acceleration.

IV. Concluding Remarks

This paper discusses a comprehensive design and set of experiments to explore the possibilities of creating a needle driver robot to fully automate the probe placement procedure during radiofrequency ablation. The robot presented here is a 1-DOF prototype that will be used and studied to help us better understand the issues related to automated probe placement, leading to a more complex multi-DOF robot that will be designed at a later stage in this project.

From the preceding discussion and results, we see that the design presented in this paper is MRI-compatible with regards to image quality, position control, and force sensing along the axis of motion. However, the faulty force readings

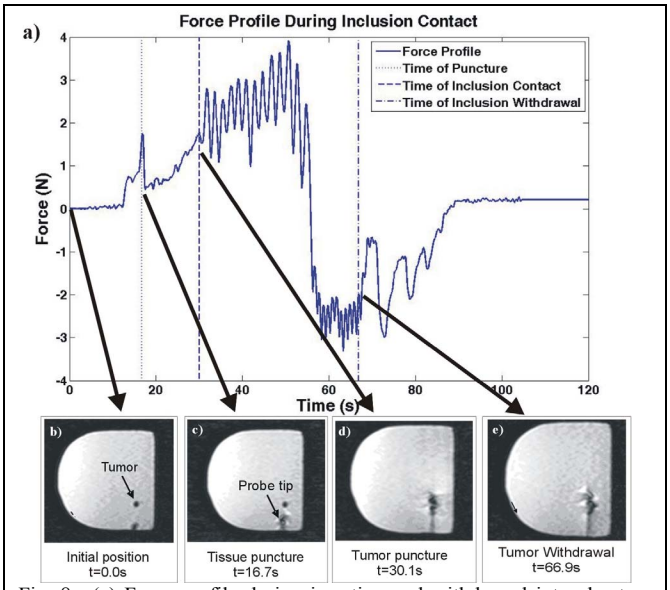

Fig. 8. (a) Force profile during insertion and withdrawal into phantom breast tissue with tumor with images from the dynamic scan, depicting (b) initial position (t = 0.0s), (c) tissue puncture (t = 16.7s), (d) tumor puncture (t = 30.1s), and (e) withdrawal from tumor (t = 66.9s).

in the y- and z-axes remain a significant limitation of the design. Solutions to the force-sensing problem will be explored in the next step of the design process and feasibility study. In addition, while preliminary studies suggest that there is a detectable difference in feedback forces during the RFA needle insertion into an inclusion, further human factors studies are required to confirm this hypothesis.

RFA under MRI is not currently as widespread as the use of RFA with ultrasound. This is primarily due to the space constraints within the magnet bore. Also, the inaccuracy of tumor localization between a biopsy and the actual RF procedure (since they are currently done on separate days) leads to registration errors and consequently inaccurate ablation boundaries. As a result, the goal of this research is to be able to perform biopsy and RFA in "one session" during continuous MRI imaging. The work presented in this paper is the first step toward the development of a robotic system with multiple degrees of freedom for RFA of tumors under continuous imaging. In future studies, a more compact robot design will be introduced with frontal access to a patient within the scanner bore, providing a safe and adequate workspace for robot operation. In addition, we are currently working on modeling the hydraulic circuit and developing a suitable controller for needle insertion. Effects of needle and soft-tissue interaction will also need to be modeled in the overall control scheme, based on our prior work on needle and soft-tissue interaction [23].

REFERENCES

1. Brown, D., *Concepts, Considerations, and Concerns on the Cutting Edge of Radiofrequency Ablation.* JVIR, 2005. **16**: p. 597-613.
2. Gazelle, G.S., et al., *Tumore Ablation with Radio-frequency Energy.* Radiology, 2000. **207**: p. 633-646.
3. Goldberg, S.N. and D.E. Dupuy, *Image-guided radiofrequency tumor ablation: Challenges and opportunities--Part 1.* JVIR, 2001. **16**: p. 1021-1032.
4. Goldberg, S.N., G.S. Gazelle, and P.R. Mueller, *A Thermal Ablation Therapy for Focal Malignancies: A Unified Approach to Underlying Principles, Techniques, and Diagnostic Imaging Guidance.* AJR, 2000. **174**: p. 323-421.
5. Yan, K. and M.H. Chen, *Radiofrequency ablation of hepatocellular carcinoma: Long-term outcome and prognostic factors.* European Journal of Radiology, 2007.
6. Earashi, M., et al., *Radiofrequency Ablation Therapy for Small Breast Cancer followed by Immediate Surgical Resection or Delayed Mammotone Excision.* Breast Cancer, 2007. **14**: p. 39-47.
7. Horiike, N., H. Iuchi, and T. Ninomiya, *Influencing factors for recurrence of hepatocellular carcinoma treated with radiofrequency ablation.* Oncology Reports, 2002. **9**: p. 1059-1062.
8. Zytoon, A., H. Ishii, and M. El-Kholy, *Recurrence-free Survival after Radiofrequency Ablation of Hepatocellular Carcinoma. A Registry Report of the Impact of Risk Factors on Outcome.* Japanese Journal of Clinical Oncology, 2007.
9. Borgert, J., et al., *Respiratory Motion Compensation with Tracked Internal and External Sensors for CT Guided Procedures.* National Institute of Health, 2005. Interventional Radiology Center.
10. Gullapalli, R., B. Zhang, and H. Richard, *MR Thermography for Radiofrequency Ablation.* JVIR, 2007. **18**(1): p. S-140.
11. Haemmerich, D. *Hepatic radiofrequency ablation -- An overview from an engineering perspective*. in *26th Ann. Int. Conf. of the IEEE EMBS*. 2004. San Francisco, CA.
12. Quaranta, V., et al., *FEM Analysis of RF Ablation: Multiprobe vs. Cool-tip electrode.* Anticancer Research, 2007. **27**: p. 775-784.
13. Stone, M. and B. Wood, *Emerging Local Ablation Technologies.* Seminars in Interventional Radiology, 2006. **23**: p. 425-438.
14. Wood, B., et al., *Technologies for Guidance of Radiofrequency Ablation in the Multimodality Interventional Suite of the Future.* JVIR, 2007. **18**: p. 9-24.
15. Solomon, S., et al., *Robotically Driven Interventions: A Method Using CT Fluoroscopy without Radiation Exposure to the Physician.* Radiology, 2002. **225**: p. 277-282.
16. Behrens, S., et al., *Computer assistance for MR based diagnosis of breast cancer: Present and future challenges.* Computerized Medical Imaging and Graphics, 2007. **31**: p. 236-247.
17. Breen, M., et al. *MRI-Guided Radiofrequency Thermal Albation: 3D Correlation of MR Lesion Images with Tissue Viability for Immediate Post-ablation Treatment Assessment*. in *25th Int. Conf. of IEEE EMBS*. 2003. Cancun, Mexico.
18. Chinzei, K. and K. Miller, *Towards MRI-Guided surgical manipulator.* Medical Science Monitor, 2001. **7**: p. 153-163.
19. Masamune, K., et al., *Development of an MRI-Compatible needle insertion manipulator for stereotactic neurosurgery.* J Image Guid Surg, 1995. **1**: p. 242-248.
20. Moser, R., et al. *An MR Compatible Robot Technology*. in *2003 IEEE Int. Conf. on Robotics & Automation*. 2003. Taipei, Taiwan.
21. Yu, N. and R. Riener, *Review of MRI-Compatible Robotic Systems*, in *Int. Conf. on Biomedical Robotics and Biomechatronics*. 2006. p. 661-665.
22. Hidler, J., et al., *MR compatible force sensing system for real-time monitoring of wrist moments during fMRI testing.* Journal of Neuroscience Methods, 2006. **155**: p. 300-307.
23. Hing, J., A. Brooks, and J.P. Desai, *A Biplanar Fluoroscopic Approach for the Measurement, Modeling, and Simulation of Needle and Soft-tissue Interaction.* Medical Image Analysis, 2007. **11**: p. 62-78.